Peer-reviewed version available at Remote Sens. 2018, 10, 735; doi:10.3390/rs10050735

Article

Evaluation of Climate Change Impacts on Wetland Vegetation in Dunhuang Yangguan National Nature Reserve in Northwest China Using Landsat Derived NDVI

Feifei Pan[1]*, Jianping Xie[2], Juming Lin[2], Tingwei Zhao[2], Yongyuan Ji[3], Qi Hu[4], Xuebiao Pan[4], Cheng Wang[5], and Xiaohuan Xi[5]

[1] Department of Geography and the Environment, University of North Texas, Denton TX 76203, USA; Email: fpan@unt.edu
[2] Dunhuang Yangguan National Nature Reserve Administration and Management Bureau, Dunhuang 736200, Gansu, China; Email: 13909373373@qq.com (T. Zhao)
[3] Yangguan Museum, Dunhuang 736200, Gansu, China; Email: jiyongyuan830828@163.com
[4] College of Resources and Environmental Sciences, China Agricultural University, Beijing 100193, China; Emails: s10020292@cau.edu.cn (Q. Hu); panxb@cau.edu.cn (X. Pan)
[5] Intisture of Remoet Sensing and Digital Earth, Chinese Academy of Sciences, Beijing 100094, China; Emails: wangcheng@radi.ac.cn (C. Wang); xixh@radi.ac.cn (X. Xi)

* Correspondence: fpan@unt.edu; Tel.: +01-940-369-5109

Abstract: Based on 541 Landsat images between 1988 and 2016, the normalized difference vegetation indices (NDVIs) of the wetland vegetation at Xitugou (XTG) and Wowachi (WWC) inside the Dunhuang Yangguan National Nature Reserve (YNNR) in northwest China were calculated for assessing impacts of climate change on wetland vegetation in the YNNR. It was found that the wetland vegetation at the XTG and WWC both had shown a significant increasing trend in the past 30 years, and the increase in both annual mean temperature and peak snow depth over the Altun Mountains led to the increase of wetland vegetation. The influence of local precipitation on the XTG wetland vegetation was greater than on the WWC wetland vegetation, which demonstrates that in extremely arid regions, the major constrain to the wetland vegetation is water availability in soils which is greatly related to the surface water detention and discharge of groundwater. At both XTG and WWC, snowmelt from the Altun Mountains is the main contributor to the groundwater discharge, while local precipitation plays a less role in influencing the wetland vegetation at the WWC than at the XTG, because the wetland vegetation grows on a relatively flat terrain at the WWC, while in a stream channel at the XTG.

Keywords: wetland vegetation; normalized difference vegetation index (NDVI); Landsat; precipitation; air temperature; snowmelt; extremely arid regions

1. Introduction

Although scientists may not fully understand the natural variability of climate, one fact remains indisputable related to the current climate change, namely, that temperatures during the end of the 20th century were higher than at any time during the last millennium and the latter half of the 20th century perhaps was one of the warmest 50-year periods during the past several millennia [1-3]. The intensity and spatial distribution of precipitation also changed as a result of the increased atmospheric water vapor due to global warming [4,5], but the changes in the precipitation regime are neither spatially nor temporally uniform [6,7]. Some studies have shown that wet regions have

become wetter and dry regions have become drier [8]. It was found that precipitation increased in high latitudes in the Northern Hemisphere, and decreased in China, Australia, and the Small Island States in the Pacific Ocean. Nevertheless, climate change has produced significant impacts on almost all landscapes and ecosystems on Earth, including the wetlands [9-12].

Wetland is one of the most productive terrestrial ecosystems. As an important component of the wetland ecosystem, the wetland vegetation plays a crucial role in the ecological functions of wetland environments [13,14]; it can provide habitats for wildlife and livestock [15,16], buffer transportation and deposition of sediments, filter pollutants from contaminated water [14, 17], impact the local water and biogeochemical cycle. On the other hand, the wetland vegetation can be served as a health index of the wetland ecosystem, because the degradation of a wetland ecosystem will be directly reflected in the decreased productivity and even mortality of the wetland vegetation.

Climate change associated with increased air temperature, carbon dioxide and other greenhouse gases, and atmospheric water vapor, has and will continuously create significant impacts on the wetlands. A large amount of studies have been carried out to assess the climate change impacts on the coastal wetlands [10-12], alpine and high latitude or polar wetlands or peatlands, which are critical for storing CO_2 and other greenhouse gases [12]. However, to our knowledge, few studies have focused on the wetlands in the arid and semi-arid regions, not to mention the wetlands in the extremely arid environment, such as Dunhuang (long-term average annual precipitation <50mm) in northwest China which is the research area of this study. One possible reason is that wetlands in dry regions are very scarce, but wetlands do exist in some dry regions where the groundwater is abundant, and they play a very important role in local ecosystem, ecological function, water resources and water quality, wildlife habitat, and the population living in the areas. Therefore, this study aims to use the normalized difference vegetation index (NDVI) derived from the Landsat images in the near infrared and red channels for assessing the climate change impacts on the wetlands in the extremely arid region in northwest China. The results drawn from this study may shed some light on our understanding of climate change impacts on the wetlands in the extremely arid areas, and thereby providing the scientific basis for an effective protection and management of these precious ecosystems under current climate change.

2. Study area and data

2.1. Study area

The study area is inside the Yangguan National Nature Reserve (YNNR), located in the territory of Nanhu Township in Dunhuang City, the westernmost point of Gansu Province in China. It covers an area of 882 km^2 between 93.8833°~ 94.2833° E and 39.65°~ 40.0833° N. The YNNR is surrounded on the west, east, south and north by the Gansu Dunhuang West Lake National Nature Reserve and the Kumtag Desert, the Danghe Reservoir, the Akesa Kazak Autonomous County, and the Gobi Desert, respectively. The Nanhu oasis inside the YNNR is one of the few oases that extends westward in the northern oasis of the Qilian Mountains. In order to better protect the wetlands inside the YNNR, the Gansu Dunhuang Yangguan Nature Reserve was upgraded to a national nature reserve in 2009. In this study, two main wetlands inside the YNNR, i.e., Xitugou (XTG) and Wuwachi (WWC) are chosen for evaluating the climate change impacts on the wetland vegetation (Figure 1). The main wetland vegetation species growing in the XTG and WWC is common reed (*Phragmites australis*). In addition to the XTG and WWC, some wetlands are distributed in the northeast of the YNNR.

Preprints (www.preprints.org) | NOT PEER-REVIEWED | Posted: 28 March 2018 doi:10.20944/preprints201803.0233.v1

Peer-reviewed version available at Remote Sens. 2018, 10, 735; doi:10.3390/rs10050735

However, since these wetlands belong to a different watershed, they are not selected in this study. The majority of the green areas shown in Figure 1 actually are vineyards, orchards, and crop fields, which are not wetlands, and thus they are also not selected in this study.

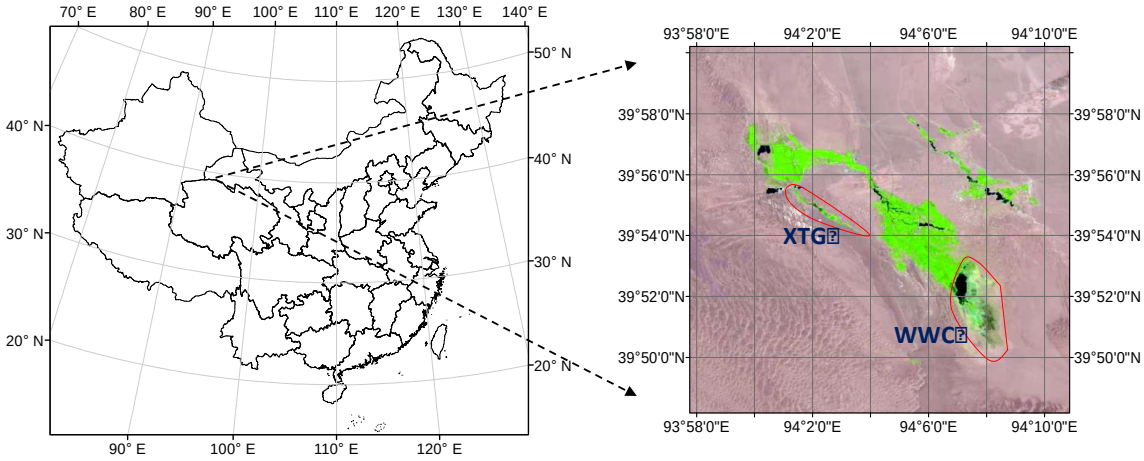

Figure 1. shows the locations of the Yangguan National Nature Reserve (YNNR) in Gansu Province of China, and two wetlands inside the YNNR: Xitugou (XTG) and Wowachi (WWC).

2.2. Meteorological data

Since climate is a long-term average of weather or meteorological elements, to study the climate change impacts on the wetland vegetation inside the YNNR, a long-term record of the meteorological data over the YNNR is essential for exploring climatic characteristics and climate change in the YNNR. The main meteorological variables include temperature, precipitation, air pressure, vapor pressure (or relative humidity), wind speed and direction. Although there is an automatic weather station installed in Wuwachi (39.87°N, 94.11°E), it started hourly collecting metrological data since 2011 and stopped working in 2013. The hourly meteorological data can be used to compute daily mean temperature, precipitation and mean wind speed. However, this automatic weather station could only provide a three-year meteorological data record which is too short for studying the climate characteristics and climate change in the YNNR.

To solve the lack of a long-term meteorological data in the YNNR, this study utilized Dunhuang weather station (40.15°N, 94.68°E), which is the closest weather station to the YNRR and has a long-term meteorological data record. The Dunhuang weather station is about 60 km northeast of the YNRR, and can provide more than 60 years (from 1951 to current) of meteorological data including daily mean, maximum, and minimum temperatures, precipitation, wind speed, vapor pressure and etc. To demonstrate that the meteorological data collected by the Dunhuang weather station can be used to study the climatic characteristics of the YNRR, this study first compared the temperature and precipitation collected by the Dunhuang weather station and the WWC automatic weather station. Based on the actual operational period of the WWC automatic weather station, we compared monthly mean temperature and monthly precipitation from April 2011 to December 2013 and plotted them in Figure 2. Since there are many missing temperature data in February, April, and May of 2012 at the WWC automatic weather station, monthly mean air temperatures of these three months are not shown in Figure 2.

Preprints (www.preprints.org) | NOT PEER-REVIEWED | Posted: 28 March 2018 doi:10.20944/preprints201803.0233.v1

Peer-reviewed version available at Remote Sens. 2018, 10, 735; doi:10.3390/rs10050735

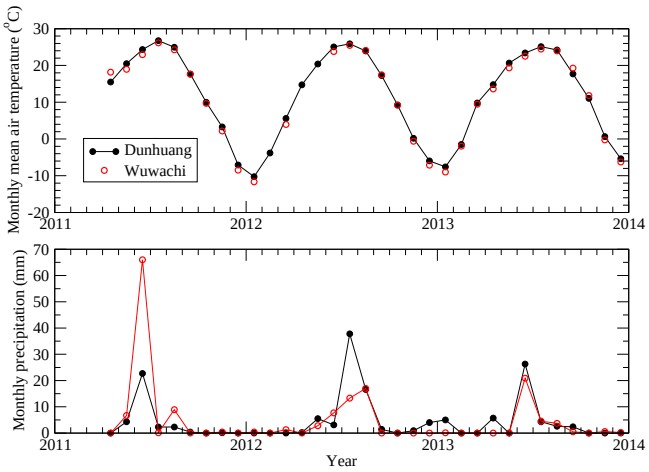

Figure 2. Time series plots of monthly mean air temperature and monthly precipitation measured at the Dunhuang weather station and the WWC automatic weather station.

Figure 2 shows that monthly mean air temperature and monthly precipitation at Wuwachi were highly (the correlation coefficient is 0.997) and fairly (the correlation coefficient is 0.667) correlated with those at Dunhuang, respectively. Although the correlation coefficient of the monthly precipitation between Wuwachi and Dunhuang is not as high as that of monthly mean air temperature, the occurrence of precipitation at Wuwachi actually corresponded well with that at Dunhuang, and among 33 months (from April of 2011 to December of 2013), there are only three months when Wuwachi received no precipitation while Dunhuang received more than 1 mm precipitation. The above comparison indicates that the long-term metrological data collected at the Dunhuang weather station are suitable for exploring the climatic characteristics and climate change in the YNNR.

2.3. The hydrologic regime of the YNNR

The hydrologic regime of the YNNR is directly influenced by the climatic and terrain characteristics of the area. According to the precipitation data collected at the Dunhuang weather station, the long-term (1951-2016) average annual precipitation in the YNNR is less than 50 mm, which is much less than the annual precipitation threshold for defining an arid climate, i.e., 250mm, and thus the study area can be classified as an extremely arid area with extremely limited surface water. The channel networks (blue lines) and watershed divides (red lines) shown in Figure 3 indicate that the surface water flow in the YNNR is from south to north, although the surface runoff in the area is very limited because of the very limited precipitation. Almost all channels in the area are dry without any water, except during the snowmelt season. Majority of the snowmelt coming from the snow cover over the Altun Mountains (~ 5000m above mean sea level) to the south of the YNNR recharges into the local groundwater systems and flows northward, and eventually emerges in the YNNR specially at the WWC and XTG (see Figure 3) as springs which provide precious water for the wetlands in the WWC and XTG. Therefore, to study the climate change impacts on the wetland vegetation in the YNNR, in addition to the local meteorological data, snow depth or snow water equivalent information in the Altun Mountains is also essential. In this study, the Canadian Meteorological Centre (CMC) operational global daily snow depth analysis data [18] with a spatial resolution of 24km were downloaded from the National Snow and Ice Data Center for evaluating the

temporal variation of the snow depth in the Altun Mountains and its impact on the wetland vegetation in the YNNR.

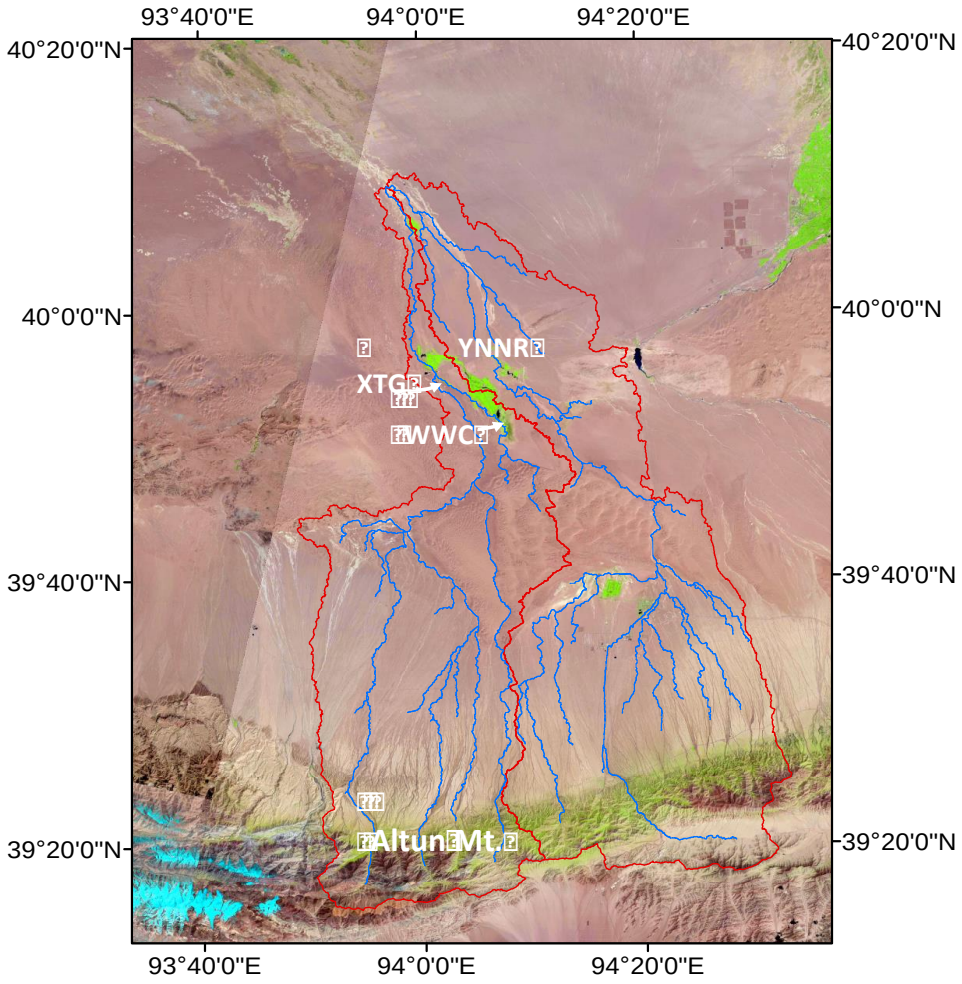

Figure 3. The hydrologic regime of the YNNR. Blue lines are channel networks, and red lines are watershed divides.

2.4. Landsat imagery

Since the XTG in the YNNR is a narrow channel and the channel width ranges from 50m to 200m (see Figure 1 and Figure 3), and thus the MODIS vegetation characteristic data products with spatial resolutions of 250m, 500m, and 1000m are not suitable for studying the wetland vegetation in the XTG. The MODIS data probably work well for the wetland vegetation in the WWC. But for the consistency, this study only used the Landsat imagery for estimating the normalized difference vegetation index (NDVI). From 1988 to 2016, 453 scenes of Landsat 5 Thematic Mapper (TM) images (path=137, row=32) and 88 scenes of Landsat 8 Operational Land Imager (OLI) images (path=137, row=32) were download from the United States Geological Survey (USGS) EarthExplorer website. All images are in the Level-1 GeoTIFF data format.

Preprints (www.preprints.org) | NOT PEER-REVIEWED | Posted: 28 March 2018 doi:10.20944/preprints201803.0233.v1

Peer-reviewed version available at Remote Sens. 2018, 10, 735; doi:10.3390/rs10050735

3. Methods

3.1. Computing the normalized difference vegetation index (NDVI)

In this study, both Landsat 5 Thematic Mapper (TM) and Landsat 8 Operational Land Imager (OLI) images were utilized for computing the normalized difference vegetation index (NDVI), which is a ratio of the spectral reflectance difference between the near-infrared and red bands to the reflectance summation of the near-infrared and red bands as shown in Eq.(1):

$$NDVI=\frac{R_{NIR}-R_{RED}}{R_{NIR}+R_{RED}} \quad (1)$$

where R_{NIR} and R_{RED} are the spectral reflectance in the near-infrared and red bands, respectively. Table 1 lists the band index and the wavelength (λ) information for the near-infrared and red bands of Landsat 5 TM and Landsat 8 OLI.

Table 1. Landsat spectral bands used for computing NDVI.

	Landsat 5 TM		Landsat 8 OLI	
	Band Index	λ(μm)	Band Index	λ(μm)
Red:	Band 3	0.626-0.693	Band 4	0.636-0.673
NIR:	Band 4	0.776-0.904	Band 5	0.851-0.879

Prior to computing NDVI based on Eq.(1), each pixel's digital number (DN) of Landsat red and NIR band images need to be converted to the spectral reflectance. For Landsat 5, we need first to convert DN to the spectral radiance as follows:

$$\boldsymbol{L_\lambda = DN_\lambda \times G_\lambda + B_\lambda} \quad (2)$$

where L_λ is the spectral radiance [W/(m² sr μm)], DN_λ is the digital number [dimensionless], G_λ is rescaling gain factor [W/(m² sr μm)], and B_λ is the rescaling bias factor [W/(m² sr μm)] for band λ. Table 2 lists the band-specific rescaling factors for Landsat 5's band 3 and band 4 [19].

Table 2. Band-specific recalling factors for Landsat 5 band 3 and band 4.

	G_λ [W/(m² sr μm)]	B_λ [W/(m² sr μm)]
Band 3	1.043976	-2.21
Band 4	0.876024	-2.39

After the spectral radiance $\boldsymbol{L_\lambda}$ is converted from the digital number, it can be used to compute the top-of-atmosphere (TOA) reflectance $\boldsymbol{R_\lambda}$ [dimensionless] as follows:

$$\boldsymbol{R_\lambda = \frac{\pi L_\lambda d^2}{ESUN_\lambda cos\theta}} \quad (3)$$

Preprints (www.preprints.org) | NOT PEER-REVIEWED | Posted: 28 March 2018 doi:10.20944/preprints201803.0233.v1

Peer-reviewed version available at Remote Sens. 2018, 10, 735; doi:10.3390/rs10050735

where d is the Earth-Sun distance in astronomical units, $\boldsymbol{ESUN_\lambda}$ is the mean solar exoatmospheric irradiance [W/(m² μm)] for band λ ($\mathbf{ESUN_\lambda}$: $\mathbf{Band3 = 1536}$, $\mathbf{Band4 = 1031}$), $\boldsymbol{\theta}$ is the solar zenith angle which is given in the metadata file of each Landsat scene. Chander et al. [19] produced a table of the Earth-Sun distance for the day of the year (DOY) using the Jet Propulsion Laboratory Ephemeris (DE405). Table 3 lists 24 Earth-Sun distances (d) of 24 DOYs, which can be used to interpolate the Earth-Sun distance (d) of the DOY that is not listed in Table 3.

Table 3. Earth-Sun distance in astronomical units

DOY	d	DOY	d	DOY	d	DOY	d
1	0.9832	91	0.9993	196	1.0165	288	0.9972
15	0.9836	106	1.0033	213	1.0149	305	0.9925
32	0.9853	121	1.0076	227	1.0128	319	0.9892
46	0.9878	135	1.0109	242	1.0092	335	0.9860
60	0.9909	152	1.0140	258	1.0057	349	0.9843
74	0.9945	166	1.0158	274	1.0011	365	0.9833

For Landsat 8 OLI imagery, the digital number DN can be directly converted to TOA reflectance as follows:

$$R_\lambda = (DN_\lambda \times M_\lambda + A_\lambda)/cos\theta \quad (4)$$

where M [dimensionless] and A [dimensionless] are rescaling factors for converting DN to reflectance in band $\boldsymbol{\lambda}$, and $\boldsymbol{\theta}$ is the solar zenith angle in degree which is given in the metadata file of each Landsat scene. The conversion of TOA reflectance from Landsat 8 OLI DN has been simplified, since all bands have the same M and A values, i.e., $M = 2 \times 10^{-5}$, *A=-0.1*.

3.2. Trend and correlation analyses

To detect if there exists a temporal trend in a variable Y, such as climatic components (e.g., air temperature, precipitation, vapor pressure, wind speed, snow depth) or vegetation characteristics (e.g., NDVI, leaf area index), a linear equation can be used to fit the time series plot of Y versus time. If it is the annual time series, the linear regression equation is given as follows:

$$\boldsymbol{Y = at + b} \quad (5)$$

where *t* is the year index (t=1, 2, …, n), n is the sample size, *a* is the annual trend slope, and *b* is the intercept. Both *a* and *b* can be determined using the least squares method. Multiplying the estimated annual trend rate by 10 yields the decadal trend rate, i.e., *10a*.

To evaluate if there exists a strong correlation between two variables *X* and *Y*, the correlation coefficient between *X* and *Y* can be calculated as follows:

$$r = \frac{\sum_{i=1}^{n}(x_i-\bar{X})(y_i-\bar{Y})}{\sqrt{\sum_{i=1}^{n}(x_i-\bar{X})^2 \sum_{i=1}^{n}(y_i-\bar{Y})^2}} \quad (6)$$

Preprints (www.preprints.org) | NOT PEER-REVIEWED | Posted: 28 March 2018 doi:10.20944/preprints201803.0233.v1

Peer-reviewed version available at Remote Sens. 2018, 10, 735; doi:10.3390/rs10050735

where r is the correlation coefficient between X and Y, i is the data index (i =1,…,n), n is the sample size, $\overline{X}$ and $\overline{Y}$ are means of x and y, respectively.

4. Results and Discussion

4.1. Climatic characteristics of the YNNR

The climatic characteristics of the YNNR can be revealed by the long-term (1951-2016) meteorological data collected at the Dunhuang weather station. During 1951-2016, the average annual mean air temperature is 9.78°C, and the average annual precipitation is 36 mm, which is much less than 250mm (the threshold for classifying a desert climate). Using the same 66 years of data, we computed the long-term average monthly mean air temperature, monthly precipitation, monthly mean atmospheric vapor pressure, and monthly mean wind speed, and plotted them in Figure 4. During the past 66 years, monthly mean temperature, monthly precipitation, and monthly mean vapor pressure all exhibited the same pattern which was high in summer and low in winter. The highest monthly mean temperature, monthly precipitation, and monthly mean vapor pressure were 25.06°C, 11.39mm, and 12.71 hpa, respectively, and all occurred in July; while the lowest monthly mean temperature and vapor pressure were -8.56°C and 1.66 hpa in January, while the lowest monthly precipitation happened in February and was 0.27mm. The monthly mean wind speed was high in spring and low in fall, i.e., 2.61m/s in April, and 1.52m/s in October. The extremely limited annual precipitation and seasonal precipitation in the growing season (May-August) indicate that the local precipitation and surface water in the YNNR could not sustain the growth of the wetland vegetation in this area, and snowmelt and groundwater must be the main water supply for the wetland vegetation growing in the YNNR wetlands.

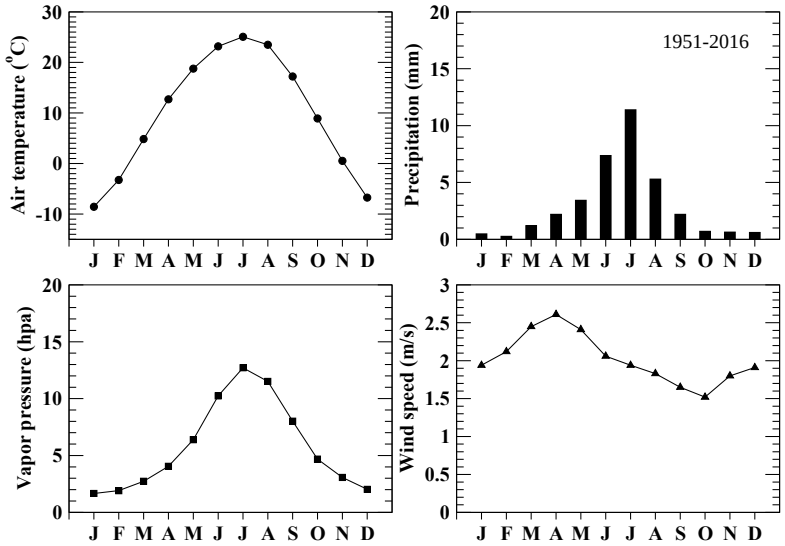

Figure 4. Monthly mean air temperature, monthly precipitation, monthly mean vapor pressure and wind speed.

4.2. Climate change in the YNNR

According to the fifth assessment report produced by the Intergovernmental Panel on Climate Chang (IPCC, 2013), the earth's climate has warmed globally by approximately 0.72 °C [0.49-0.89]

over the past 60 years, and the decade of the 2000s has been the warmest period compared to any other decades since the late 19th century. To investigate the temperature change in the YNNR, the time series plot of the annual mean temperature in the YNNR and the best fit of the time series plot were shown in Figure 5, which demonstrate that the temperature in the YNNR had exhibited a significant ($p<0.01$) increasing trend with a decadal rate of 0.23°C/decade (or 1.38°C/ 6 decades), which is almost twice of the global average temperature increase in the past six decades, i.e., 0.72°C (IPCC< 2013). The annual mean temperature anomaly plotted in Figure 5 shows that during the past 20 years (since 1997), the annual mean temperature anomaly was always positive, and thus the temperature increase in the paste 20 years was the most significant and the strongest. These results are consistent with the IPCC's report (IPCC, 2013).

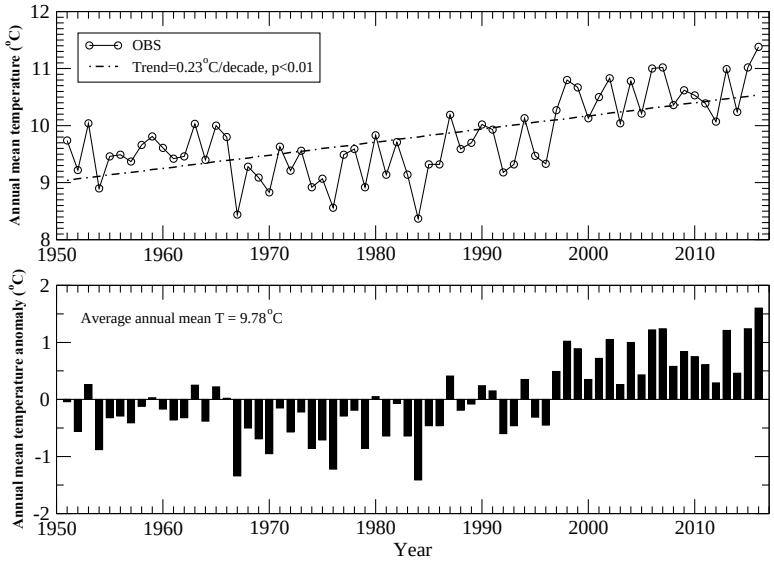

Figure 5. The time series plot of the annual mean temperature and the best fit line (top); the annual mean temperature anomaly plot (bottom).

Figure 6 shows that the annual precipitation in the YNNR during 1951-2016 exhibited a significant increasing trend ($p<0.01$) with a growth rate of 4.50mm/decade. According to the annual precipitation anomaly illustrated in Figure 6, we can find that the largest positive anomaly occurred in 1979, which caused the flood in the Danghe River to the east of the YNNR. Since 1990 there were six positive anomalies greater than 20 mm, and they occurred in 1993, 1995, 2002, 2007, 2012, and 2016, respectively. In the period of 1950-1970, annual precipitation showed almost continuous negative anomalies, indicating that the climate in the YNNR in the 1950s and 1960s was drier than in the past two decades. Combined with the change of annual mean temperature and precipitation during 1951-2016, we can find that the climate in the YNNR exhibited a tendency of warming and "wetting", but the annual precipitation in the YNNR was still much less than 250mm (the threshold for classifying a desert climate), which means that the precipitation regime in the YNNR has not changed fundamentally, and it is still extremely dry.

Preprints (www.preprints.org) | NOT PEER-REVIEWED | Posted: 28 March 2018 doi:10.20944/preprints201803.0233.v1

Peer-reviewed version available at Remote Sens. 2018, 10, 735; doi:10.3390/rs10050735

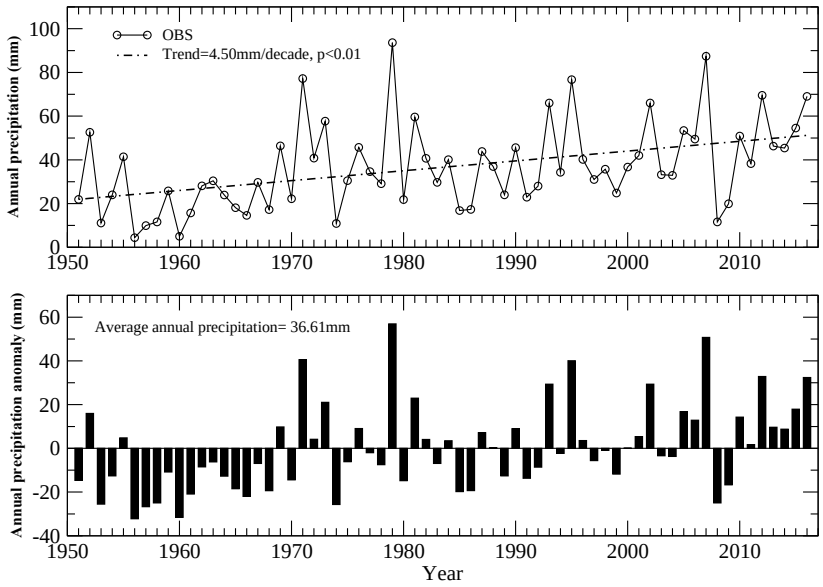

Figure 6. The time series plot of annual precipitation and the best fit line (top); and annual precipitation anomaly plot (bottom).

In order to gain a better understanding of the climate change in the YNNR, Figure 7 shows the long-term average monthly mean temperature and monthly precipitation during the period of 1951-2016. In additional to the long-term average, the decadal average monthly mean temperature and monthly precipitation in each decade (1951-1959, 1960-1969, 1970-1979, 1980-1989, 1990-1999, 2000-2009, 2010-2016) were also calculated and plotted in Figure 7. According to Figure 7, monthly mean temperature in the YNNR basically exhibited a continuously increasing trend (i.e., 2000s > 1990s > 1980s > 1970s > 1960s > 1950s) in every month, and it was particularly noticeable between March and August. However, unlike monthly mean temperature, monthly precipitation in the YNNR showed irregular changes without a consistent increasing or decreasing pattern. The monthly precipitation in summer months (June, July and August) usually had the largest variations, and the main reason probably is that precipitation events in the YNNR mainly occurred in summer months.

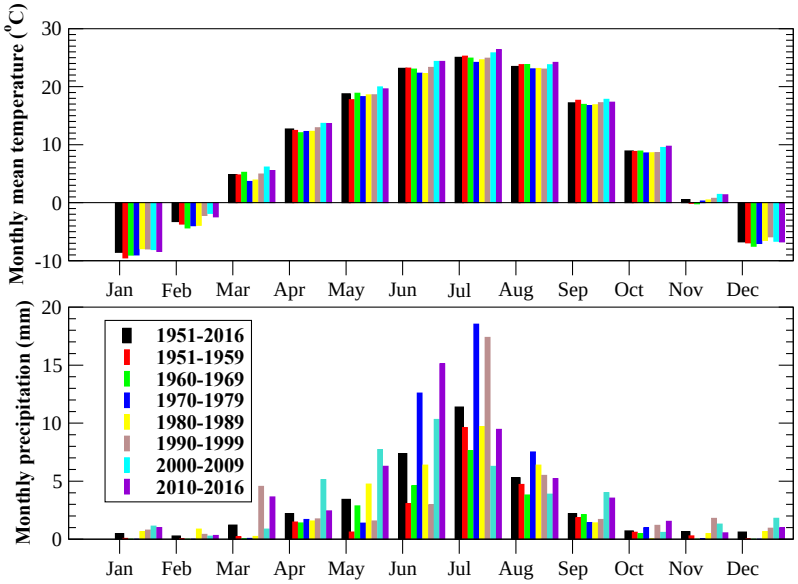

Figure 7. Long-term and decadal averages of monthly mean temperature (top) and monthly precipitation (bottom).

Preprints (www.preprints.org) | NOT PEER-REVIEWED | Posted: 28 March 2018 doi:10.20944/preprints201803.0233.v1

Peer-reviewed version available at Remote Sens. 2018, 10, 735; doi:10.3390/rs10050735

4.3. Analysis of the Landsat derived NDVI of the wetland vegetation in the YNNR

To evaluate climate change impacts on the wetland vegetation in the YNNR, we first used the methods described in section 3.1. to compute NDVI based on near-infrared and red band images of each of 541 downloaded Landsat scenes (453 Landsat 5 TM and 88 Landsat 8 OLI images). As an example, Figure 8 shows the computed NDVI in the YNNR on July 26, 2016 from Landsat 8 OLI near-infrared and red band images. According to Figure 8, even at the peak of the growing season, NDVI of the majority of the area is less than 0.1 because of the Gobi Desert. The areas with NDVI > 0.5 are orchards, vineyards, and crop fields. Areas in the XTG and WWC as marked in Figure 8 showing NDVI >0.4 are associated with the wetland vegetation.

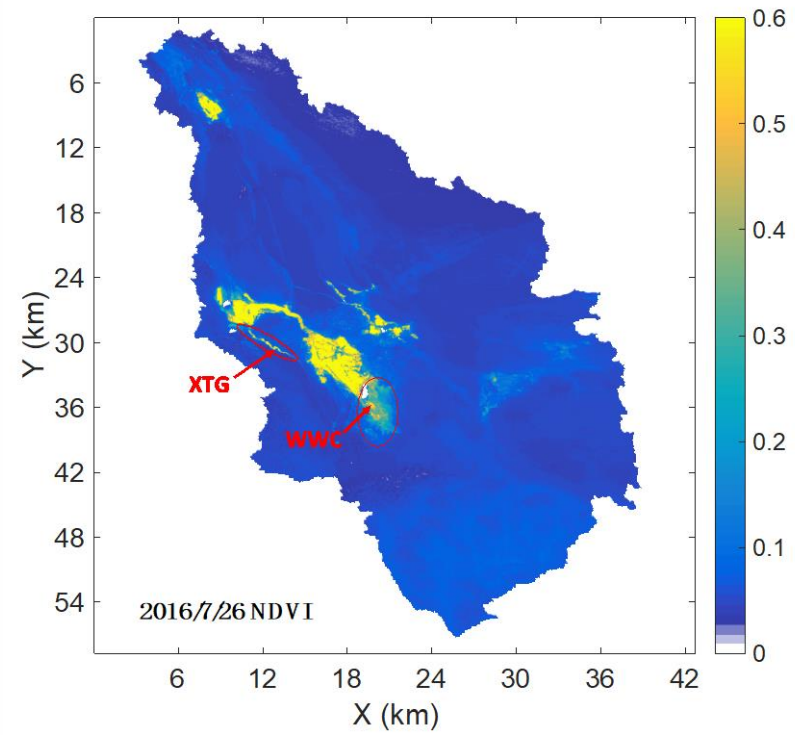

Figure 8. NDVI on July 26, 2016 computed from Landsat 8 OLI near infrared and red band images.

Based on 541 NDVI images derived from Landsat 5 TM and Landsat 8 OLI images, we identified one pixel (30m×30m) each in the XTG and WWC areas with the highest occurrence frequency of the maximum NDVI inside each circle as shown in Figure 8. The selected pixels are considered as the typical wetland vegetation pixels in the XTG and WWC, which are pointed by the arrows in Figure 8. The time series plots of the computed NDVIs of these two pixels are shown in Figure 9. During the growing seasons, some very low NDVIs shown in Figure 9 are due to clouds.

Preprints (www.preprints.org) | NOT PEER-REVIEWED | Posted: 28 March 2018 doi:10.20944/preprints201803.0233.v1

Peer-reviewed version available at Remote Sens. 2018, 10, 735; doi:10.3390/rs10050735

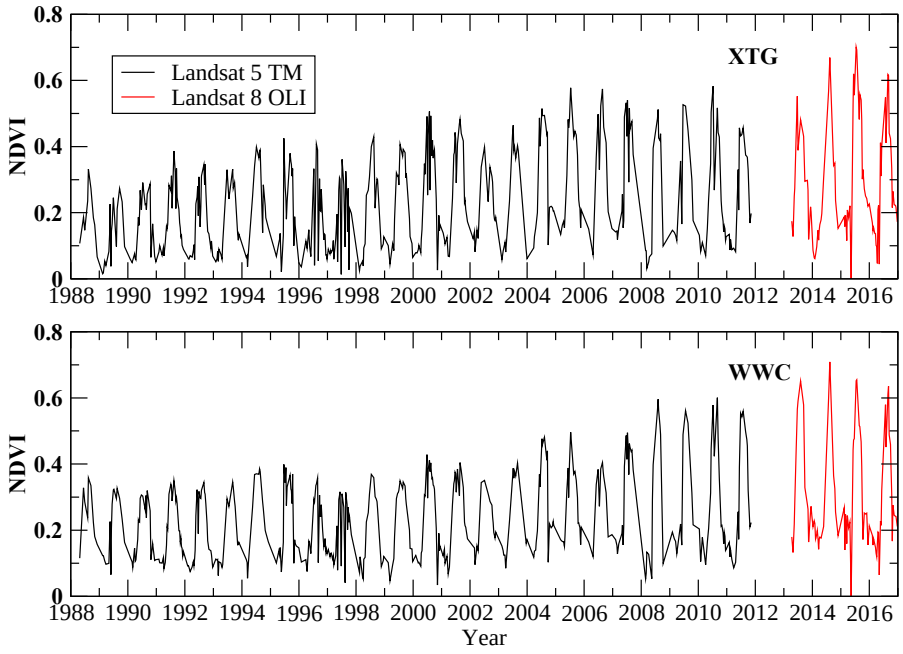

Figure 9. The times series of the computed DNVIs of one pixel in the XTG (top) and one pixel in the WWC (bottom).

According to Figure 9, the wetland vegetation in the XTG and WWC both exhibited an increasing trend, especially during the past 20 years, which is clearly reflected in the peak NDVI values. Therefore, it is better to conduct the trend and correlation analyses of the peak NDVI values rather than the whole computed NDVIs. The time series plots of the peak NDVIs at the XTG and WWC are plotted in Figure 10. Using the trend analysis method, a significant increasing trend was detected for the peak NDVIs at the XTG (0.12/decade, $p<0.01$) and WWC (0.13/decade, $p<0.01$) during the last 30 years. The difference in the magnitude of the peak NDVI growth rate between the XTG and WWC over the past 30 years is only 0.01/decade, which is insignificant.

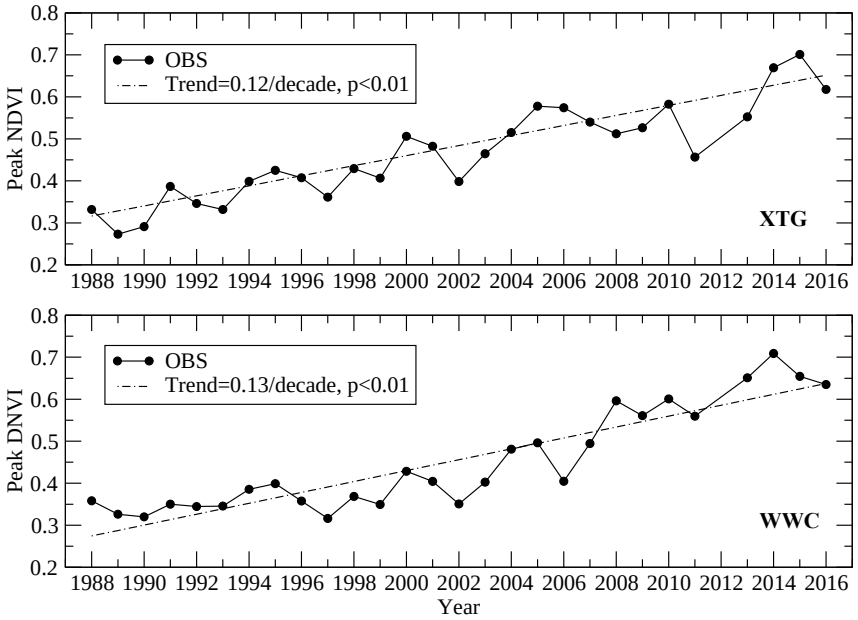

Figure 10. The time series plots of the peak NDVIs and the best fit lines at the XTG (top) and the WWC (bottom).

4.4. Climate change impacts on the wetland vegetation in the YNNR

As results shown in section 4.2, the climate in the YNNR during the past 60 years has exhibited a significant warming trend in the annual mean temperature (trend=0.23°C/decade, $p<0.01$), and a significant "wetting" trend in the annual precipitation (trend=4.5mm/decade, $p<0.01$). To correlate the climate change in the YNNR with the temporal variation of the wetland vegetation at the XTG and WWC, we first employed the trend analysis to extract the trends in the annual mean temperature and annual precipitation during the past 30 years, since the computed NDVIs in this study are from 1988 to 2016. It was found that from 1988 to 2016, the annual mean temperature displayed a significant increasing trend with a rate of +0.48°C/decade ($p<0.01$) which is more than double of the trend (+0.23°C/decade) during the past 60 years, and the annual precipitation also showed a significant increasing trend with the same rate as the past 60 years (i.e., +4.5mm/decade, $p<0.01$). The results indicate that during the past 30 years, the climate warming in the YNNR has intensified, while the precipitation regime has not changed significantly, because the annual precipitation in the YNNR had only increased at a very low rate, i.e. +4.5mm/decade. Using the correlation analysis method as described in section 3.2, we computed the correlation coefficients (r) between the peak NDVI and annual mean temperature and annual precipitation and listed the results in Table 4.

Table 4. Correlation coefficients (r) between the peak NDVI and annual mean temperature and annual precipitation at the XTG and WWC between 1988 and 2016

	XTG	WWC
Annual mean temperature	0.65	0.53
Annual precipitation	0.27	0.16

The results shown in Table 4 indicate that the increased annual temperatures in the YNNR played a significant role in the peak NDVI growth of the wetland vegetation at the XTG (r=0.65) and the WWC (r=0.53) during 1988-2016. However, the increase in precipitation (+4.5mm/decade, $p<0.01$) contributed little to the wetland vegetation growth in the YNNR. Comparing the XTG and WWC, we can find that the impact of precipitation on the wetland vegetation at the XTG (r=0.27) is greater than that on the wetland vegetation at the WWC (r=0.16). This is because of the fact that the wetland vegetation at the XTG is mainly grown in the stream channel (known as the XTG, see Figure 3) with water retention and thus the surface runoff generated by precipitation is collected in the XTG which has a direct impact on and contribution to the XTG's wetland vegetation. While the wetland vegetation growing at the WWC is distributed on a relatively flat terrain (see Figure 3) with very limited water retention, and thus the local precipitation caused a less impact on the wetland vegetation at the WWC.

The photosynthesis of vegetation requires sunlight and water. The YNNR in the Gobi Desert has sufficient sunshine. Therefore, the growth of vegetation in the YNNR mainly depends on the supply of water. We know that the surface water in the YNNR is extremely scarce and the growth of vegetation primarily depends on the melting of snow from the Altun Mountains, recharging to the groundwater system and flowing from south to north beneath the surface as the groundwater flow. Part of the groundwater in the vicinity of the YNNR emerges as springs at the surface (known as seepages or spring eyes). Therefore, to study the impact of climate change on the wetland vegetation in the YNNR, changes in snow cover in the Altun Mountains and the impacts caused by the snow cover changes should also be evaluated. In this study, the peak snow depth over the Altun Mountains

Preprints (www.preprints.org) | NOT PEER-REVIEWED | Posted: 28 March 2018 doi:10.20944/preprints201803.0233.v1

Peer-reviewed version available at Remote Sens. 2018, 10, 735; doi:10.3390/rs10050735

during each snow cover season from 1999 to 2016 was extracted from the Canadian Meteorological Centre (CMC) operational global daily snow depth analysis data [18] (the CMC snow depth data is only available from 1999 to current). Based on the period of the CMC snow depth data, we re-assessed the trend values of each variable including the peak snow depth during the past 20 years (i.e., 1999-2016) and plotted them in Figure 11.

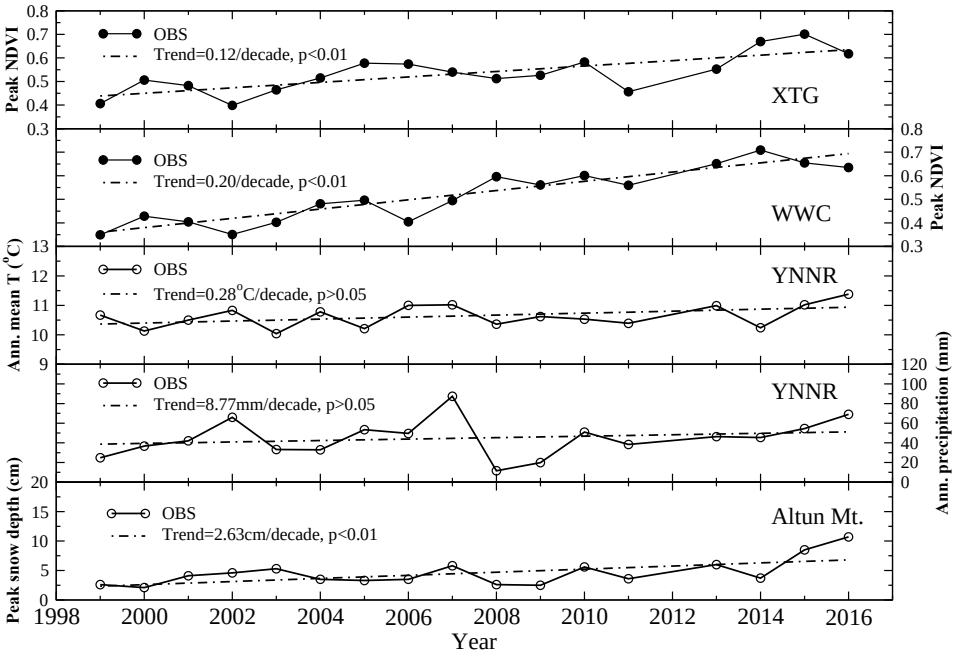

Figure 11. The time series plots of the peak NDVIs at the XTG and WWC, annual mean temperature and annual precipitation in the YNNR, and the peak snow depth over the Altun Mountains during 1999-2016, and the best fit lines of these plots.

Figure 11 shows that the annual peak NDVIs at the XTG and WWC during the last 20 years both exhibited a very significant increase trend ($p<0.01$), while at the XTG the increasing rate during the past 20 years was identical to that during the past 30 years (i.e., 0.12/decade), and at the WWC the trend rate from 1999 to 2016 was about 1.54 times of that during the past 30 years, which indicates that the wetland vegetation growth at the WWC became faster during the past 20 years than that at the XTG. With regard to the controlling factors, the annual mean temperature and annual precipitation both displayed an insignificant ($p>0.05$) increasing trend at a rate of +0.20° C/decade and +8.77mm/decade, respectively, while the annual peak snow depth over the Altun Mountains showed a significant increasing trend (2.63cm/decade, $p<0.01$). The correlation coefficients between the annual peak NDVIs and the climatic controlling factors are listed in Table 5.

Table 5. Correlation coefficients (r) between the peak NDVIs and annual mean temperature and annual precipitation in the YNNR, and annual peak snow depth in the Altun Mt. during 1999-2016

	XTG	WWC
Annual mean temperature	0.25	0.17
Annual precipitation	0.30	0.06
Annual peak snow depth	0.49	0.42

The results listed in Table 5 demonstrate that during the past 20 years, the major contributor to the wetland vegetation growth at the XTG and WWC is the increased annual peak snow depth in the Altun Mountains (r=0.49 at the XTG, and r=0.42 at the WWC). The correlation coefficient between annual precipitation and the annual peak NDVIs at the XTG (r=0.3) is much higher than that at the WWC (r=0.06), which proves that the local precipitation plays a stronger role in the wetland vegetation at the XTG than at the WWC, because the wetland vegetation at the XTG grows in the stream channel and the WWC's wetland vegetation is distributed on a flat terrain (see Figure 3). During the past 20 years, the contribution of the increased annual mean temperature to the wetland vegetation at the XTG and WWC both decreased by more than 30% compared to the past 30 years, i.e., at the XTG, r=0.25 for the past 20 years, and r=0.65 for the past 30 years; at the WWC, r=0.17 for the past 20 years, and r=0.53 for the past 30 years.

According to Table 5, during the past 20 years the impacts due to climate change on the wetland vegetation growth at the XTG are greater than at the WWC, because the correlation coefficients between the peak NDVIs at the XTG and climatic variables (i.e., annual mean temperature, annual precipitation and annual peak snow depth) are all larger than those at the WWC. However, the annual peak NDVI increasing rate at the XTG actually is less than that at the WWC by 0.08/decade, which indicates that the wetland vegetation at the XTG (close to several tourism sites) is more fragile and susceptible to human activities than the wetland vegetation at the WWC (not close to any tourism sites and has less influence from human activities). On the other hand, some effective wetland protection measures (e.g., prohibition of grazing, annual prescribed burning) for the wetland vegetation at the WWC implemented by the Dunhuang Yangguan Nature Reserve Administration and Management Bureau also played an important role in the increase of the wetland vegetation at the WWC.

5. Conclusions

To study the climate change impacts on the wetland vegetation in the Dunhuang Yangguan National Nature Reserve (YNNR) (39°39′-40°05′N, 93°53′- 94°17′E) in Gansu Province of China, about 541 Landsat 5 TM and Landsat 8 OLI images between 1988 and 2016 were used to compute the normalized difference vegetation indices (NDVIs) of the wetland vegetation (mainly reed) at the Xitugou (XTG) and Wowachi (WWC) inside the YNNR. It was found that the wetland vegetation at the XTG and WWC both had shown a significant increasing trend in the past 20-30 years. The difference in the annual peak NDVI growth rate of the wetland vegetation at the XTG between the past 20 years and 30 years is insubstantial, while the annual peak NDVI growth rate of the wetland vegetation at the WWC during the past 20 years was about 1.5 times of the past 30 years. The increase in the annual mean temperature in the past 20 years combined with the increase in annual peak snow depth over the Altun Mountains led to the increase of the wetland vegetation at the XTG and WWC. The contribution of snowmelt to the increase of the wetland vegetation in the YNNR was higher than the contribution from the temperature rise. The influence of the local precipitation on the wetland vegetation at the XTG was far greater than that at the WWC, since the XTG's wetland vegetation mainly grows in the confluence area of stream channel with a larger flow accumulation area, while the WWC's wetland vegetation grows on a large flat area. Although the correlation coefficients of

annual mean temperature, annual precipitation, annual peak snow depth over the Altun Mountains and the annual peak NDVI of the XTG's wetland vegetation are all higher than the corresponding correlation coefficients of the WWC's wetland vegetation in the recent 20 years, the increasing rate of the annual peak NDVI peak at the XTG in the recent 20 years is about 0.08 less than that of the wetland vegetation at the WWC, which indicates that the wetland vegetation at the XTG (which is close to several tourism sites) is more fragile and thus more vulnerable to human activities than the wetland vegetation at the WWC (which is not close to any tourism sites and has less influence from human activities). In addition, some effective wetland protection measures (e.g., prohibition of grazing, annual prescribed burning) for the WWC's wetland vegetation implemented by the Dunhuang Yangguan Nature Reserve Administration and Management Bureau during the past 20 years also contributed to the increase of the wetland vegetation at the WWC.

This study demonstrates that in extremely arid regions such as the YNNR with an average annual precipitation less than 50 mm, the major constrain to the wetland vegetation is water availability in soils which is greatly related to the surface water detention and discharge of groundwater. At both XTG and WWC, snowmelt from the Altun Mountains is the main contributor to the groundwater discharge, while local precipitation plays a less important role in influencing the wetland vegetation at the WWC than that at the XTG, because the wetland vegetation grows on a relatively flat terrain at the WWC, while in a stream channel at the XTG.

References

1. Bradley, R.S. Past global changes and their significance for the future. *Quaternary Science Reviews*. **2000**, *19*, 391-402.
2. Bradley, R.S. 1000 years of climate change. *Science*. **2000**, *288*, 1353-1355.
3. Luterbacher, J.; Dietrich, D.; Xoplaki, AE.; Grosjean, M.; Wanner, H. European seasonal and annual temperature variability, trends, and extremes since 1500. *Science*. **2004**, *303*, 1499-1503.
4. O'Gorman, P.A.; Schneider, A. The physical basis for increases in precipitation extremes in simulations of 21st-century climate change. *Proceedings of the National Academy of Sciences of the United States of America.* **2009**, *106(35)*, 14773-14777.
5. Trenberth, K.E. Attribution of climate variations and trends to human influences and natural variability. *Wiley Interdisciplinary Reviews Climate Change*. **2011**, *2(6)*, 925–930.
6. Walther, G.R.; Post, E.; Convey, P.; Menzel, A.; Parmesan, C.; Beebee, T.J.; Fromentin, J.M.; Hoegh-Guldberg, O.; Bairlein, F. Ecological responses to recent climate change. *Nature.* **2002**, *416(6879)*,389-395.
7. Frich, P.; Alexander, L.V.; Della-Marta, D.; Gleason, B.; Haylock, M.; Klein Tank, A.M.G.; Pelerson, T. Observed coherent changes in climatic extremes during the second half of the twentieth century. Climate Research. **2002**, *19*, 193-212.
8. Wentz, F.J.; Ricciardulli, L.; Hilburn, K.; Mears, C. 2007. How much more rain will global warming bring? *Science*. **2007**, *317(5835)*, 233-235.
9. Dore, M.H. 2005. Climate change and changes in global precipitation patterns: what do we know? *Environment International*. **2005**, *31(8)*, 1167-1181.
10. Erwin, K.L. Wetlands and global climate change: the role of wetland restoration in a changing world. *Wetland Ecology and Management*. **2009**, 17, 71-84.
11. Scavia, D.; Field, J.C.; Boesch, D.F.; Buddemeier, R.W.; Burkett, V.; Cayan, D.R.; Fogarty, M.; Harwell, M.A.; Howarth, R.W.; Mason, C.; Reed, D.J.; Rover, T.C.; Sallenger, A.H.; Titus, J.G. Climate change impacts on U.S. coastal and marine ecosystems. Estuaries. **2002**, *25*, 149-164.
12. Burkett, V.; Kusler, J. Climate change: potential impacts and interactions in wetlands of the United States, *Journal of the American Water Resources Association*. **2000**, *36*, 313-320.
13. Adam, E.; Mutanga, O.; Rugege, D. Multispectral and hyperspectral remote sensing for identification and mapping of wetland vegetation: a review. *Wetlands Ecology and Management*. **2010**, *18(3)*, 281-296.

14. Silva, T.S.; Costa, M.P.; Melack, J.M.; Novo, E.M. Remote sensing of aquatic vegetation: theory and applications. *Environmental monitoring and assessment*. **2008**, *140(1-3)*, 131-145.
15. Mutanga, O.; Adam, E.; Cho, M.A. High density biomass estimation for wetland vegetation using WorldView-2 imagery and random forest regression algorithm. *International Journal of Applied Earth Observation and Geoinformation*. **2012**, 18, 399-406.
16. Owino, A.O.; Ryan, P.G. Recent papyrus swamp habitat loss and conservation implications in western Kenya. *Wetlands Ecology and Management*. **2007**, *15(1)*, 1-12.
17. Huang, J.; Wang, S.; Yan, L; Zhong, Q. Plant photosynthesis and its influence on removal efficiencies in constructed wetlands. *Ecological Engineering*. **2010**, *36(8)*, 1037-1043.
18. Brown, R.D.; Brasnett, B. Canadian Meteorological Centre (CMC) Daily Snow Depth Analysis Data, 2017, Version 1. NASA National Snow and Ice Data Center Distributed Active Archive Center, Boulder, Colorado, USA.
19. Chander, G; Markham, B.L.; Helder, D.L. Summary of current radiometric calibration coefficients for Landsat MSS< TM, ETM+, and EO-1 ALIO sensors. *Remote Sensing of Environment*. **2009**, *113*, 893-903.